Operation Planning of an Independent Microgrid for Cold Regions by the Distribution of Fuel Cells and Water Electrolyzers Using a Genetic Algorithm

Shin'ya Obara*, Seizi Watanabe**, Balaji Rengarajan***

*Power Engineering Laboratory, Department of Electrical and Electronic Engineering, Kitami Institute of Technology

165 Koen-cho, Kitami, Hokkaido 090-8507, Japan

E-mail: obara@mail.kitami-it.ac.jp

**Department of Mechanical Engineering, Kushiro National College of Technology

Otanozhike 2-32-1, Kushiro, Kokkaido 084-0916, Japan

E-mail: seiji@mech.kushiro-ct.ac.jp

***Centre for Fuel cell technology, International Advanced Research Centre for Powder Metallurgy and New Materials

IIT-M Research Park, Phase-1, Second Floor, 6, Kanagam Road, Taramani, Chennai 600 113, India

E-mail: balaji.energy@gmail.com

Abstract

An energy system using a microgrid was examined in this work. The motivations for this study are to promote green energy usage, discuss concerns regarding energy supply during disasters, and improve the efficacy of waste heat usage. To create a society based on clean hydrogen energy, this paper studied the use of a microgrid to supply energy to six houses in a cold region. The proposed microgrid consisted of photovoltaics, a water electrolyzer, a fuel cell, and a heat pump; furthermore, this microgrid was not accompanied by any external energy supply. In this paper, the optimized

calculation results obtained from the genetic algorithm (GA) were compared between a system operated using one set of large capacity equipment (a concentrated system) and a system operated using two or more pieces of distributed small capacity equipment (a distributed system). From this comparison, the operation efficiency of each set of equipment was characterized using the difference in the load factor of the fuel cell and that of the water electrolyzer of each system. Moreover, the optimal capacities of the solar cell, fuel cells, water electrolyzers, and heat pumps while operating an energy-independent microgrid with the concentrated system and the distributed system were presented.

Keywords: Independent microgrid, Cold regions, Distributed fuel cell, Water electrolysis, Genetic algorithm

1. Introduction

Integrating distributed energy resources can reduce power transmission losses, improve the efficacy of waste heat usage, and utilize green energy. To promote the spread of green energy, improve the method of supplying energy in times of disaster, and utilize waste heat more efficiently, a distributed energy system using a microgrid was examined in this study [1-3]. The energy supply system in the microgrid does not require equipment to be installed in all of the houses in the microgrid. Therefore, a distributed energy system has lower equipment cost than a standalone system due to the centralization of equipment. The goal of this paper was to model a society based on clean hydrogen energy by considering the operation of an independent microgrid in cold regions. The microgrid consisted of fuel cells, heat pumps, and water electrolyzers that used photovoltaics. Until now, only compound systems consisting of photovoltaics and water electrolyzers have been investigated [4-6]. The dynamic characteristics of a system with photovoltaics and a compound

water electrolyzer were investigated [7, 8], and an analysis and physical testing of those optimizations [9] were reported. Distributing the energy equipment within a microgrid is simple, and the selection of the type and capacity of the pieces of equipment is flexible. In this paper, a microgrid was operated by one set of large-scale fuel cells as a concentrated system. In contrast, a distributed system consists of two or more small-capacity fuel cells. Because the load factors of the fuel cell for each system differ when they are introduced into a microgrid with large power load changes, the power generation efficiency is also expected to differ. Similarly, the installation capacity for the water electrolysis equipment is expected to affect the production efficiency. The production efficiency of hydrogen and oxygen differs between a concentrated system and a distributed system.

This paper discusses the construction of an independent microgrid that uses only the electric power of photovoltaics. In addition, the relationship between the load factor and efficiency of each piece of equipment placed in the microgrid is investigated using a numerical analysis that utilizes a genetic algorithm (GA). In the proposed system, the electricity demand and thermal demand of an entire microgrid were satisfied using the electric power obtained from two or more arrays of photovoltaics. Hydrogen and oxygen were generated by distributed water electrolyzers using the surplus power from the photovoltaics. These storage gases were supplied to a proton-exchange membrane fuel cell (PEFC) at an arbitrary time. Two or more electric heat pump systems were introduced into a proposed microgrid assuming that the proposed system would be installed in cold regions with a high thermal energy demand. Moreover, because the electric power of the photovoltaics could be stored by a water electrolyzer, an expensive battery was not installed in the proposed system. In an energy-independent microgrid using photovoltaics, optimizing the area of the solar cell is important. Furthermore, it is necessary to clarify the differences in the operation method between a concentrated system and a distributed system for a fuel cell and a water electrolyzer. Therefore, the construction of an independent microgrid for cold regions supplied only with the electric power of photovoltaics is dependent upon two factors: the equipment capacities and

the operation plan for both the concentrated system and the distributed system. Furthermore, the partial load performances of a fuel cell and a water electrolyzer were considered for both the concentrated and distributed systems.

2. Proposed Microgrid

2.1 System schematic

Figure 1 depicts the system flow of an independent microgrid with solar water electrolysis. This microgrid supplies electric power and heat to six houses in total. Figure 2 explains the details of these load characteristics. As shown in Fig. 1, the electric power obtained by the photovoltaics (photovoltaics (1) to (4)) can be supplied to a power grid, the heat pumps (heat pumps (1) and (2)), and the water electrolyzers (water electrolyzers (1) to (3)). In this paper, the operation of one set of large-scale equipment (as in a concentrated system) and the operation of a distribution of two or more small-capacity sets of equipment (as in a distributed system) were investigated. Hydrogen and oxygen produced by a water electrolyzer were stored in their respective cylinders using compressors. The volumes of a hydrogen cylinder and an oxygen cylinder at 1 MPa are 2 and 1 m^3, respectively. The gas stored in each cylinder could be supplied to a fuel cell (PEFC (1) to (3)) at an arbitrary time. The PEFCs and the water electrolyzers used in the distributed system were placed in three locations labeled (1) to (3). The concentrated system consisted of one set of fuel cells and one set of water electrolyzers. Accordingly, the fuel cells PEFC (1) to (3) and the water electrolyzers (water electrolysis (1) to (3)) for the concentrated system in Figure 1 (a) were combined into one set of equipment.

Figure 1 (b) shows the schematic representation of a heat supply system. The waste heat from a PEFC was stored in a heat storage tank. An ethylene glycol water solution was used as a thermal

storage medium. When the heat demand of the microgrid exceeded the capacity of the heat storage facility, the required heat was supplied by the heat pump.

2.2 Energy balance of the system

Equations (1) and (2) depict the balance equations for the electric power and heat of the proposed microgrid shown in Fig. 1, respectively. The left-hand and right-hand sides of each equation are input terms and output terms, respectively. The terms $E_{needs,t}$ and $H_{needs,t}$ from the right-hand side of each equation are the electricity demand and the thermal demand, respectively. In this paper, the energy-loading pattern shown in Fig. 2 was used [10]. The load pattern of Fig. 2 shows the average daily value measured in a standard house in Sapporo, Japan for 1 year. An electric light and household appliances comprised the power load. The load for space heating, water heating and for heating the warm water of a bathtub comprised the thermal load The subscript t under each equation referred to the sampling time. The fuel cell, photovoltaics, electrolytic cell, and heat pump could be configured as one set (for a concentrated system) or as two or more sets (for a distributed system). The output of solar cells from photovoltaics (1) to (3) was supplied to the water electrolyzer through a DC-DC converter (labeled DC-DC converter (1)). Otherwise, the output of the solar cells was supplied to heat pumps (1) and (2), then to a microgrid through a DC-DC converter (2), and finally to an inverter. Conversely, the output of fuel cells PEFC (1) to (3) was supplied to the heat pumps and a microgrid through a DC-DC converter (2) and an inverter. Therefore, when distributing a fuel cell and the photovoltaics to a distant location, the distributed installation of DC-DC converters and inverters is required. Furthermore, it is necessary to consider the auxiliary power consumption of machines including a compressor (E_{CP}) for the hydrogen and oxygen produced from water electrolysis and a blower (E_{BW}). Air from the blower was used for the cathode of the PEFC and for cooling the water electrolyzer. However, the pump power required to circulate the hot water in a microgrid was not included in the power balance Eqs. (1-1) and (1-2). This pump

power was omitted because the power consumption of the pump is strongly influenced by the route (distance) of the hot water. Equation (1-1) expresses the case in which the output of the photovoltaics is supplied to a microgrid; in contrast, Eq. (1-2) represents the case in which the output of the photovoltaics is supplied to the water electrolyzer. A heat loss accompanying the heat input and output of the heat storage tank was considered. Therefore, the efficiency of thermal storage ($\eta_{HST,in}$) and the efficiency of heat output ($\eta_{HST,out}$) from the heat storage tanks are introduced in Eq. (2).

$$\left(\sum_{i=1}^{N_{FC}} E_{FC,i,t}\right)\cdot\eta_{dc2}\cdot\eta_{it}+\left(\sum_{j=1}^{N_{PV}} E_{PV,j,t}\right)\cdot\eta_{dc2}\cdot\eta_{it}=E_{needs,t}+\sum_{l=1}^{N_{HP}} E_{HP,l,t}+E_{BW,2,t} \tag{1-1}$$

$$\begin{aligned}&\left(\sum_{i=1}^{N_{FC}} E_{FC,i,t}\right)\cdot\eta_{dc2}\cdot\eta_{it}+\left(\sum_{j=1}^{N_{PV}} E_{PV,j,t}\right)\cdot\eta_{dc1}\\&=E_{needs,t}+\sum_{k=1}^{N_{EL}} E_{EL,k,t}+\sum_{l=1}^{N_{HP}} E_{HP,l,t}+\sum_{m=1}^{N_{CP}} E_{CP,m,t}+\sum_{n=1}^{N_{BW}} E_{BW,n,t}\end{aligned} \tag{1-2}$$

$$\sum_{i=1}^{N_{FC}} H_{FC,i,t}+\sum_{j=1}^{N_{HP}} H_{HP,j,t}+H_{HST,t-1}\cdot\eta_{HST,out}=H_{needs,t}+H_{HST,t}\cdot\eta_{HST,in} \tag{2}$$

2.3 Equipment Characteristics

2.3.1 Water electrolyzer

For the work in this paper, a hydrogen generator [11] with a proton-exchange membrane that was developed by Rengarajan et al. was used. Figure 3 (a) shows the experimental results of running the water electrolyzer with a load factor L_f and energy efficiency η_{EL} as described above reference [11]. Equations (3) and (4) define the potential efficiency η_{ELe} and the current efficiency η_{ELi}, respectively. Energy efficiency η_{EL} was calculated by Eq. (5). The maximum efficiency at low loading for the hydrogen generator exceeded 90%, as represented by the efficiency of water electrolysis in Fig. 3 (a). The range of the load factor in Fig. 3 was the physical operating range of

the equipment. In the analysis described later, when the equipment load factor was less than that of the equipment shown in Fig. 3, the lower limit of each figure was used. The production efficiency of H_2 at maximum load was approximately 70%. Equation (6) was obtained when the relationship between the load factor and H_2 production efficiency shown in Fig. 3 (a) was approximated using a curve. The performance of a water electrolyzer was obtained by introducing this approximate expression into an example analysis described later.

$$\eta_{ELe} = V_{EL,th} / V_{EL} \tag{3}$$

$$\eta_{ELi} = I_{EL,g} / I_{EL,c} = G_g / G_{g,th} \tag{4}$$

$$\eta_{EL} = \eta_{ELe} \cdot \eta_{ELi} \tag{5}$$

$$\eta_{EL} = -0.00005563 \cdot L_f^3 + 0.009413 \cdot L_f^2 - 0.6617 \cdot L_f + 97.31 \tag{6}$$

2.3.2 Fuel cell

A home cogeneration system using a PEFC was sold by Japanese gas companies and oil companies in 2009. Figure 3 (b) shows the performance [13] of the home PEFC cogeneration system with 1 kW of output measured by Tokyo Gas [12]. A fuel cell system from Tokyo Gas Co Ltd. used a reformed gas for fuel by reforming natural gas, and the CO content in the reformed gas was several parts per million. Subtracting the efficiency of the fuel reformer from the total power generation efficiency of the system described above provided the curves for the power and heat generation of the PEFC in Fig. 3 (b). The partial load performance of the electric power of the PEFC without a reformer was sufficient , as shown in Fig. 3 (b). When the characteristics of the electric power and thermal power of the PEFC were approximated with curves, Equations (7) and (8) were obtained. The efficiency obtained from Eqs. (7) and (8) was the value of the outlet from a fuel cell stack. Because losses occurred regarding the electric power and heat as shown in Eqs. (1) and (2), the electric power and heat output of the system dropped rather than that calculated by Eqs. (7) and (8).

$$\eta_{FCe} = -0.002347 \cdot L_f^2 + 0.3534 \cdot L_f + 29.01 \tag{7}$$

$$\eta_{FCh} = -0.0010893 \cdot L_f^2 + 0.239 \cdot L_f + 40.54 \quad (8)$$

2.3.3 Heat pump

Figure 3 (c) shows the relationship between the load factor and the coefficient of performance (COP) of an air-source heat pump (a standard heat pump currently produced commercially in Japan) introduced into the proposed microgrid. The data were collected at an outdoor air temperature of 20 °C and a hot water temperature of 65 °C. When the heat pump was operated at less than 70% of the load factor, the COP decreased rapidly. The relationship between this heat pump and the load factor could be expressed by an approximate expression in Eq. (9).

$$COP_{HP} = 0.00000270 \cdot L_f^3 - 0.0008107 \cdot L_f^2 + 0.08129 \cdot L_f + 0.8794 \quad (9)$$

2.3.4 Photovoltaics

Figure 4 shows the solar position (in Fig. 4 (a)) and the amount of insolation (Fig. 4 (b)) in 2008 on representative days in January and July in Sapporo, Japan [14]. The amount of insolation on a level surface and a sloped surface is shown in Fig. 4 (b). The insolation on the sloped surface was calculated as the amount of insolation incident onto a plate inclined at an angle of 30 degrees in the southern direction. The electricity produced by a solar cell and introduced into the proposed microgrid was calculated by multiplying the amount of insolation on the sloped surface of Fig. 4 (b) by the area and power generation efficiency of the solar cell. In the analysis described later, the maximum efficiency of the solar cell to generate electrical energy was set up to 20% (SANYO Electric Co., Ltd., 2011, http://us.sanyo.com/Dynamic/customPages/docs/solarPower_22_3_Cell_Efficiency_White_Paper_Dec_07.pdf).

2.3.5 Compression of hydrogen and oxygen gas

Hydrogen and oxygen produced by a water electrolyzer were pressurized and stored in cylinders. The required power of the compressor was assumed to be the work required to compress an ideal gas and was calculated using Eq. (10). The term η_{CP} in this equation was the overall efficiency of the compressor. The power consumption of an inverter and a motor, the transfer loss of mechanical power, the loss due to a gas leak and insufficient cooling, and other mechanical losses were included in η_{CP}. Accordingly, η_{CP} only included the efficiency of the gas storage input and holding processes. In the latter analysis, η_{CP} was calculated to be 0.6 (60%), assuming a real system.

$$E_{CP,H_2,t} = P_\infty \cdot U_{\infty,t} \cdot \ln(P_{CP,H_2} / P_\infty) / \eta_{CP} \tag{10}$$

3. Operation Optimization Using the GA

3.1 Chromosome model

The power output from a fuel cell and the power input to a water electrolyzer, which were both used in the balanced equation (Eq. (1)), are expressed by Eqs. (11) and (12), respectively. A fuel cell and a water electrolyzer were introduced into three sets of equipment at the maximum installation numbers. The terms α_t, β_t, and χ_t in Eq. (11)and ξ_t, ψ_t, and ζ_t in Eq. (12), respectively, are the output rates of fuel cells and the power-input rates of water electrolyzers, respectively. Here, the sums of α_t, β_t, and χ_t in sampling time t and the total of ξ_t, ψ_t, and ζ_t in sampling time t both equaled 1.0. Because the load factor of each fuel cell and each water electrolyzer changed with the set of rates, the efficiency of each piece of equipment changed.

$$\sum_{i=1}^{N_{FC}} E_{FC,i,t} = \alpha_t \cdot E_{FC,1,t} + \beta_t \cdot E_{FC,2,t} + \chi_t \cdot E_{FC,3,t} \tag{11}$$

$$\sum_{k=1}^{N_{EL}} E_{EL,k,t} = \xi_t \cdot E_{EL,1,t} + \psi_t \cdot E_{EL,2,t} + \zeta_t \cdot E_{EL,3,t} \tag{12}$$

The chromosome model used for the GA expressed each value of α_t, β_t, χ_t, ξ_t, ψ_t, and ζ_t as 0 or 1 (16 bits). The 16-bit cell value could take a total of 65,536 (=2^{16}) possible discrete steps between 0 and 1. These values were generated at random for every sampling time. Therefore, when output rates of fuel cells at all sampling times ($t = 0, 1, 2, \ldots 23$) and power input rates of water electrolyzers were calculated, the operation methods for fuel cells and water electrolyzers for the representative day could be determined. A chromosome model showing the operation method for fuel cells and water electrolyzers on a representative day described above is referred to as an individual in the GA in this paper. Figure 5 shows the configuration of the chromosome model. The rectangle outlined by broken lines in Fig. 5 is the chromosome model, which forms an individual. To maintain the diversity of an individual group in the GA, the individual N_{cr} is analyzed with each generation.

3.2 Procedure and computation expression of analysis

Table 1 shows the computation expressions that depict the operation of the proposed system by sampling time t. The relationship between the amount of heat stored and the amount of heat demanded was investigated in the first step of Table 1 to determine whether the heat pump needed to be operated. The heat pump was operated when the amount of heat demanded exceeded the amount of heat stored. In the next step, the relationship between the electricity produced by the photovoltaics and the amount of power demanded was investigated to determine whether a fuel cell or a water electrolyzer was operated. Eventually, the input and output of all the equipment was determined.

After the electric power of the photovoltaics was supplied to a power conditioner (a DC-DC converter and an inverter), it was supplied to the demand side and the heat pump to fulfill the electrical demand and the thermal demand. The surplus power in this case was used to produce hydrogen and oxygen using the water electrolyzers. When the photovoltaics could no longer produce electricity, the stored hydrogen and oxygen were supplied to the PEFC. Although the waste heat of

the PEFC in this case was used to meet the thermal demand, any excess heat was stored in a heat storage tank. Because the hydrogen, oxygen, and heat storage tanks were included in the proposed system, it was necessary to plan the operation such that the energy equations (Eqs. (1) and (2)) could be balanced based on the amount of hydrogen stored ($Q_{H_2,ST,t-1}$) and the amount of heat stored ($H_{HST,t-1}$) during the sampling time. For this reason, the quantities of hydrogen, oxygen, and heat at the time $t-1$ during the beginning of an operation strongly influenced the subsequent operational plan. Furthermore, because the electric power demand and the available photovoltaic power changed with the sampling time, the time of begin of an operation also influenced the operational plan for the system. Therefore, in this study, the amount of hydrogen stored (the residual quantity) at the final time ($t=23$) for 1 day became the initial value at the beginning of the operation ($t=0$) for the next day. As a result, the proposed system could be continuously managed during the representative month.

3.3 Objective function

Operation of the proposed system began at 0:00 of a representative day, and the system controller managed the operating plan until 23:00 that day. The amount of hydrogen stored in the system at $t=0$ and $t=23$ were $Q_{H_2,ST,0}$ and $Q_{H_2,ST,23}$, respectively. Equation (13) is the objective function of the proposed system. The solution that fulfilled this objective function is a solution of high fitness. The penalty factor in this GA method was given when the energy balance of Eq. (1) and (2) were not satisfied. Moreover, as shown in Eq. (13), the objective function was given to allow the amount of hydrogen to be balanced by the amount obtained by a water electrolyzer in 1 day. Hydrogen was produced with electric power, which was more expensive than heat. Therefore, the priority was to balance the electric energy and the amount of hydrogen by the method proposed in this analysis.

$$\left| Q_{H_2,ST,23} - Q_{H_2,ST,0} \right| \rightarrow \text{minimize} \quad (\text{Here,} \quad Q_{H_2,ST,23} \geq Q_{H_2,ST,0}) \ . \tag{13}$$

3.4 Analysis flow

3.4.1 Computational procedure for the energy balance equations

Figure 6 shows the analysis flow for optimizing the proposed system using the GA. First, analysis conditions, such as the areas of the solar cells, and the solution parameters of the GA were entered into a computer. Then, the numerous chromosome models described in Section 3.1 were generated at random by the computer. The power output $E_{FC,i,t}$ of each PEFC and power input $E_{EL,l,t}$ of each electrolyzer in sampling time t were decided by decoding these chromosome models using α_t, β_t, and χ_t and ξ_t, ψ_t, and ζ_t in Eqs. (11) and (12), respectively. When the power output of each PEFC was determined, the amount of the PEFC waste heat ($H_{FC,i,t}$) for the number i in time t could be obtained using the load factors of the fuel cells in Eq. (8) and the loads of each fuel cell. The thermal power $H_{HP,j,t}$ requested from the heat pumps was obtained using $H_{FC,i,t}$, the heat demand $H_{needs,t}$, and the heat stored $H_{HST,t-1}$ during time $t-1$ in Eq. (2). The load factor was calculated using $H_{HP,j,t}$, which was described above, and the capacity of the heat pump. The COP was decided from the relationship between this load factor and Fig. 3 (c). The power consumption $E_{HP,l,t}$ of each heat pump could subsequently be obtained from the COP calculated above ($E_{HP,l,t} = H_{HP,j,t}/COP$). If the amount of electricity $E_{PV,j,t}$ produced by each set of photovoltaics, the amount of power demand $E_{needs,t}$, and the power consumption $E_{EL,l,t}$ of each water electrolyzer are known, then the power consumption $E_{CP,m,t}$ of the hydrogen and oxygen compressors can be obtained from Fig. 4, the power consumption $E_{BW,n,t}$ of the blowers can be

introduced into Eq. (1), and the energy stored by hydrogen and oxygen $Q_{H_2,ST,t}$ can be calculated. Therefore, $Q_{H_2,ST,t}$ was calculated from the power $E_{EL,l,t}$ supplied to the water electrolyzers and the relationship between the load factor and the efficiency of the water electrolyzer, the latter of which is shown in Fig. 3 (a). Equation (14) is the formula for $Q_{H_2,ST,t}$, and Eq. (15) is the amount of hydrogen generated $q_{H_2,t}$. Here, e_w is the enthalpy of water formation.

$$Q_{H_2,ST,t} = Q_{H_2,ST,t-1} + q_{H_2,t} \tag{14}$$

$$q_{H_2,t} = 0.0224 \cdot \left(\sum_{l=1}^{N_{EL}} E_{EL,l,t} \Big/ e_w \right) \cdot \eta_{EL} \tag{15}$$

The analysis presented in Fig. 6 revealed an equal number of chromosomes and planned operation methods. According to the value of the objective function (Eq. (13)), individual groups were arranged in order according to the results of these operational plans. To maintain the diversity of these individuals, the genetic manipulation of crossover and mutation was added under a probability given ahead of time to the high-ranking individuals (the elitism method). The crossover operation of a chromosome model includes the operation described below. Based on the probability given beforehand, one set of parent chromosomes (two individuals) was chosen at random. Furthermore, the crossover positions in the parent chromosomes were determined at random, and the genes in each parent chromosome were exchanged. The choromosome mutation model proceeded by choosing an individual at random under the probability given beforehand, choosing a gene at random, and replacing 0 and 1. It is made to increase by the elitism method such that the first and the second ranking chromosome may include 30% of all of the chromosome models, and the chromosome model of the third to the fifth ranking could include 10% of the models. The predetermined number of generations was found by repeating the calculation described above. The solution for the final generation was defined as the optimal solution.

3.4.2 Concentrated system and distributed system

The schematic representation of the system introduced into a microgrid for cold regions was investigated with an example analysis consisting of a concentrated system and a distributed system. A fuel cell and a water electrolyzer were introduced into a concentrated system. Two cases were studied for the distributed system. The first case introduced one fuel cell and a set of three water electrolyzers. This system was referred to as a D-A system. The second case introduced a set of three fuel cells and a set of three water electrolyzers. This system was referred to as a D-B system. The total capacity of the distributed a set of three fuel cells and the distributed a set of three water electrolyzers was the same as the total capacity of one set in the centralized system. The effect of the distributed energy equipment could be determined by comparing the concentrated system, the D-A system, and the D-B system. The capacities of the three fuel cells and the three water electrolyzers were equally divided, respectively. . Moreover, the relationships between the load factors and the efficiencies of a fuel cell and a water electrolyzer were assumed to follow Figs. 3 (a) and 3 (b) without being dependent on the capacity of each component. Here, the division capacitance is defined as individual capacity rating.

3.5 Analysis condition and equipment capacity

Table 2 shows the specification, the efficiency, and power consumption of each component used in the proposed system. The capacity of a heat storage tank and the volume of the cylinders of hydrogen and oxygen were not shown because they were obtained from the results of the operation analysis. When the flow from Fig. 6 was calculated to balance the energy balance equations (Eqs. (1) and (2)), the minimum capacities of the fuel cells, the water electrolyzers, the heat pump, and the minimum area of the solar cell could be obtained. These values were determined by investigating the minimum of each value when balancing the energy balance equations. Subsequently, the GA searched for the minimum capacity of each piece of equipment at or below 100% of the load factor.

However, the equipment capacities required in winter, when the most energy was needed (January), were used for the calculations throughout the year because the electricity produced and the energy demand from the photovoltaics changed between months. As a result, the total capacities of the fuel cells and water electrolyzers were 30 and 105 kW, respectively. The assumed maximum power load of the system determined the equipment capacity. Because the amounts of insolation differed, the total areas of the solar cells differed greatly between January and July. The areas of the solar cells required in January and July were 346 and 76 m^2, respectively. These values were the required maximum monthly values obtained from the analysis of the system. Because the area of the solar cells required in January was used in the example analysis, the area was set to 346 m^2. Therefore, an electric power surplus occurred in the summer. Because the total capacity of the heat pump in winter needed to be 100 kW, the required equipment with a total capacity of 100 kW was introduced into the proposed microgrid. Table 3 shows the variables used for the GA.

Each value in Table 3 was determined by applying a trial-and-error method repeatedly to the analytical calculation. To maintain the diversity of the chromosome model, a high number of chromosome models and a high probability of crossover and mutation were used. As a result, the convergence value could be obtained with a small generation number.

4. Analysis Results

4.1 Operation efficiencies of the fuel cell and the water electrolyzer

(1) Operation efficiency of a fuel cell

Figure 7 shows the analysis results of the energy balance of the system. Below, the operation analysis details of the system are examined. Figure 8 shows the analysis of output efficiencies for the operation of the fuel cells and the water electrolyzers that were introduced into the concentrated system in January and July. The time interval during which the efficiency was zero for each month gave the electricity demand for the photovoltaics. As shown in Fig. 3 (b), the efficiency of the fuel cell increased as the load factor increased. In contrast, the efficiency of the water electrolyzer decreased

as the load factor increased, as shown in Fig. 3 (a). For this reason, the load factor of a fuel cell in January was high because of the high heat energy demand in January (winter) compared to that in July (summer). Moreover, the efficiency of the fuel cell in January was high compared to that in July. Based on the characteristics of Fig. 3 (a), the average load factor of the water electrolyzer in January was high compared to that in July, and the efficiency of the electrolyzer in July was high compared to that in January.

Figures 9 and 10 show the analysis results for the efficiency of a fuel cell and a water electrolyzer introduced into the distributed system (D-A system (Fig. 9) and D-B system (Fig. 10)). The characteristics of the power generation efficiency of the fuel cell shown in Figs. 8 (a), 9 (a), and 10 (a) were similar when the results of July for the D-B system (Fig. 10 (a)) were excluded. The time that the fuel cell was operated in July for the D-B system was 3 h lower than that for the other systems. This was because the operation of distributed PEFCs with high load factors could be planned. Although the fuel cell was introduced into the concentrated system and the D-A system was a single set, the fuel cell was distributed as three sets in the D-B system. Therefore, distributing the fuel cells could decrease the required operation hours of the equipment for a month with a low load factor.

(2) Operation efficiency of the water electrolyzer

Although the operation times of the water electrolyzer of the concentrated system (Fig. 8 (b)) and the D-A system (Fig. 9 (b)) were the same, the efficiency of the D-A system was better. In contrast, the operation time of the water electrolyzer in the D-B system in July (Fig. 10 (b)) was 3 h lower than that of the other systems. Because the total efficiency improves with the distribution of fuel cells, less heat was wasted. For this reason, the thermal power of the heat pumps using electric power from the photovoltaics was increased. Because the surplus power of the photovoltaics decreased because less electric power was supplied to the water electrolyzer, the operation time of the water electrolyzer decreased. Moreover, the efficiency of the D-B system in January increased.

The difference between the efficiency of the water electrolyzers in the D-A system and the D-B system could be explained as follows. Because the fuel cell was not distributed in the D-A system, the efficiency drop during the partial load was large. Therefore, the load on the heat pump decreased because the exhaust heat of a fuel cell increased. However, the decrease in the efficiency of the D-B system under the partial load was less than the D-A system because the fuel cell of the D-B system was distributed. There was little heat lost from the fuel cell. As a result, the COP of the heat pump in the D-B system became higher than that in the D-A system because the load factor of the fuel cell increased with the operation of the heat pump.

4.2 COP of the heat pump

Figure 11 shows the analysis results for the COP of the heat pump in the concentrated system, the D-A system, and the D-B system. The results for January, a month with high thermal demands, were similar for all of the systems. In contrast, the results in July for the D-B system differed greatly from those of the other two systems. As described in Section 4.1 (2), operation of the D-A system was accompanied by a decline in efficiency due to the partial load of the fuel cell. As a result, the amount of heat lost from the fuel cell increased, and the load on the heat pump decreased. However, there were fewer efficiency drops in the D-B system due to partial load than there were in the D-A system because the fuel cells in the D-B system were distributed. Therefore, little heat was lost from the fuel cells, and the load factor of the heat pump output increased. As a result, the COP of the D-B system became higher than that of the D-A system.

4.3 Comparison of each system

Figures 12 and 13 show the daily mean load factor and the daily mean efficiency of all fuel cells and water electrolyzers on a representative day in January and July. The load factor and power generation efficiency of the fuel cells differed greatly between January and July. The efficiency of a fuel cell in each system in January improved by approximately 12% compared to that in July. The

total efficiency of the fuel cells of the D-B system in July improved by approximately 2% compared with that of the other systems. The efficiency of the water electrolyzers also differed greatly between January and July.

The load factor of the water electrolyzer in the concentrated system in January was high. Thus, the surplus power from the photovoltaics supplied to the water electrolyzer increased because the load on the heat pump decreased with the increase in waste heat as the fuel cell operated at a partial load. In the concentrated system, which introduced a single set consisting of a fuel cell and a water electrolyzer, a drop in the power generation efficiency when the fuel cell operated at partial load. However, as shown in Fig. 12, the average power generation efficiency of a fuel cell for a given day hardly changed.

Figure 13 shows the results for the daily mean load factor and the daily mean power generation efficiency of the fuel cells and water electrolyzers in each system. The load factor and efficiency of the fuel cells did not differ greatly among the systems. However, the load factors of the water electrolyzers of each system differed between January and July because the efficiency characteristics of the fuel cells in each system differed under the same load. Accordingly, the operation of the distributed fuel cells (D-B system) significantly influenced the load factor of the water electrolyzer, as shown in Fig. 14.

5. Conclusions

(1) The capacity of each piece of equipment introduced into the proposed microgrid that supplied energy to six houses was determined. As a result, the total capacity of the fuel cells and water electrolyzers was 30 and 105 kW, respectively. Moreover, the area of the installed solar cells was 346 m^2 during winter (January), when there was a high energy demand. Considering the winter conditions, the system required a heat pump system with a total capacity of 100 kW.

(2) The change in the load factor and efficiency by distributing the fuel cells and the water electrolyzers was investigated. Because the fuel cell was not distributed in the concentrated system,

the drop in the efficiency during the partial load was large. Because the exhaust heat of the fuel cell increased, the load on the heat pump decreased. As the COP of the heat pump decreased with the decreasing load factor, there were time intervals in which the electric power supplied to a water electrolyzer from the photovoltaics increased. As a result, the efficiency of the water electrolyzer in the concentrated system would be lowered because the water electrolyzer frequently operated with a high load factor.

(3) For the distributed system, the operation time of the water electrolyzers was reduced by approximately 3 h for the summer compared to the time required by the concentrated system because the total power generation efficiency for the distributed fuel cells was higher than the fuel cells in the concentrated system; there was little heat lost from the fuel cells in the distributed system. For this reason, the thermal power that could be generated from the heat pump using the electric power from the photovoltaics increased. As a result, the electric power of the photovoltaics supplied to the water electrolyzers decreased and caused the operation time of the water electrolyzers to decrease.

Nomenclature

COP	:	Coefficient of performance of the heat pump
E	:	Power [W]
E_{needs}	:	Power demand [W]
e_w	:	Enthalpy of water formation [mole/h]
G_g	:	Generating gas volume [g/s]
H	:	Heat [W]
H_{needs}	:	Heat demand [W]
$I_{EL,c}$	:	Current of turning on electricity
$I_{EL,g}$	:	Contribution current of electrolysis
L_f	:	Load factor [%]

P : Pressure [MPa]

P_{∞} : Pressure of atmosphere [MPa]

$Q_{H_2,ST}$: Quantity of hydrogen storage [W]

$q_{H_2,t}$: The amount of hydrogen generation [m^3/h]

t : Sample time [h]

U_{∞} : Volume flow at atmosphere [m^3/s]

V_{EL} : Bath voltage

Greek Symbols

α , β , χ : Load rate of the distributed fuel cell

ξ_t , ψ_t , ζ_t : Power input rate of the distributed electrolyzer

η : Efficiency

η_{dc} : Efficiency of the DC-DC converter

η_{ELe} Efficiency of potential

η_{ELi} Efficiency of current

η_{it} : Efficiency of inverter

Subscripts

BW : Blower

CP : Compressor

EL : Electrolyzer

FC : Fuel cell

FC_e : Power output of the fuel cell

FC_h : Heat output of the fuel cell

HP : Heat pump

HST : Heat storage

PV : Photovoltaics

th : Theoretical

Acknowledgement

This work was partially supported by a Grant-in-Aid for the Fundamental Research Developing Association Shipbuilding Offshore (REDAS), 2010. We appreciate the support to this research by the REDAS.

References

[1] Sitthidet V., Issarachai N., Somyot K. Application of electrolyzer system to enhance frequency stabilization effect of microturbine in a microgrid system. Int J Hydrogen Energy, 2009; 34(17):7131-7142.

[2] Molina M.G., Mercado P.E. Stabilization and control of tie-line power flow of microgrid including wind generation by distributed energy storage. Int J Hydrogen Energy, 2010;35(11):5827-5833.

[3] El-Sharkh M.Y., Rahman A., Alam M.S. Short term scheduling of multiple grid-parallel PEM fuel cells for microgrid applications. Int J Hydrogen Energy, 2010;35(20);11099-11106.

[4] Bilgen E. Solar hydrogen from photovoltaic-electrolyzer systems. Energy Conversion and Management, 2001;42(9):1047-1057.

[5] Hancock Jr. O. G. A photovoltaic-powered water electrolyzer: its performance and economics. Int J Hydrogen Energy, 1986;11(3):153-160.

[6] Ganguly A., Misra D., Ghosh S. Modeling and analysis of solar photovoltaic-electrolyzer-fuel cell hybrid power system integrated with a floriculture greenhouse. Energy and Buildings, 2010;42(11); 2036-2043.

[7] Chun-Hua L., Xin-Jian Z., Guang-Yi C., Sheng S., Ming-Ruo H. Dynamic modeling and sizing optimization of stand-alone photovoltaic power systems using hybrid energy storage technology. Renewable Energy, 2009;34(3):815-826.

[8] Hwang J.J., Lai L.K., Wu W., Chang W.R. Dynamic modeling of a photovoltaic hydrogen fuel cell hybrid system. Int J Hydrogen Energy, 2009;34(23):9531-9542.

[9] Thomas L. Gibson, Nelson A. Kelly, Optimization of solar powered hydrogen production using photovoltaic electrolysis devices. Int J Hydrogen Energy, 2008;33(21): 5931-5940.

[10] Narita K., The research on unused energy of the cold region city and utilization for the district heat and cooling. Ph. D. thesis, Hokkaido University, Sapporo; 1996.

[11] Rengarajan B., et al. Development and performance evaluation of proton exchange membrane (PEM) based hydrogen generator for portable applications. Int J Hydrogen Energy, 2011;36(2): 1399-1403.

[12] http://www.tokyo-gas.co.jp/index_e.html, 2011.

[13] http://www.iae.or.jp/publish/kihou/28-2/04.html, 2005.

[14] NEDO Technical information data base, Standard meteorology and solar radiation data (METPV-3), http://www.nedo.go.jp/database/index.html, 2009.

Captions

Fig. 1 System outline

Fig. 2 Power and heat demand model in Sapporo, Japan

Fig. 3 Characteristics of each component

(a) Efficiency of the water electrolysis

(b) Efficiency of the PEFC

(c) COP of the heat pump

Fig. 4 Insolation of the level surface in Sapporo

(a) The direction of the solar angle and elevation

(b) Solar insolation

Fig. 5 Chromosome model using GA

Fig. 6 Analysis flow using GA

Fig. 7 Analysis results of the energy balance of the system

(a) Balance of electric power

(b) Balance of heat

Fig. 8 Analysis results of efficiency in centralized system

(a) Fuel cell

(b) Electrolyzer

Fig. 9 Analysis results of the efficiency of the D-A system

(a) Fuel cell

(b) Electrolyzer

Fig. 10 Analysis results of the efficiency of the D-B system

(a) Fuel cell

(b) Electrolyzer

Fig. 11 The COP results of the heat pumps

(a) Central system

(b) D-A system

(c) D-B system

Fig. 12 Analysis results of the fuel cell

(a) January

(b) July

Fig. 13 Analysis results of the electrolyzers

(a) January

(b) July

Fig. 14 Analysis results of the daily average

Table 1 Computation equations used for analysis

Table 2 Specification of each component

Table 3 Parameters of GA

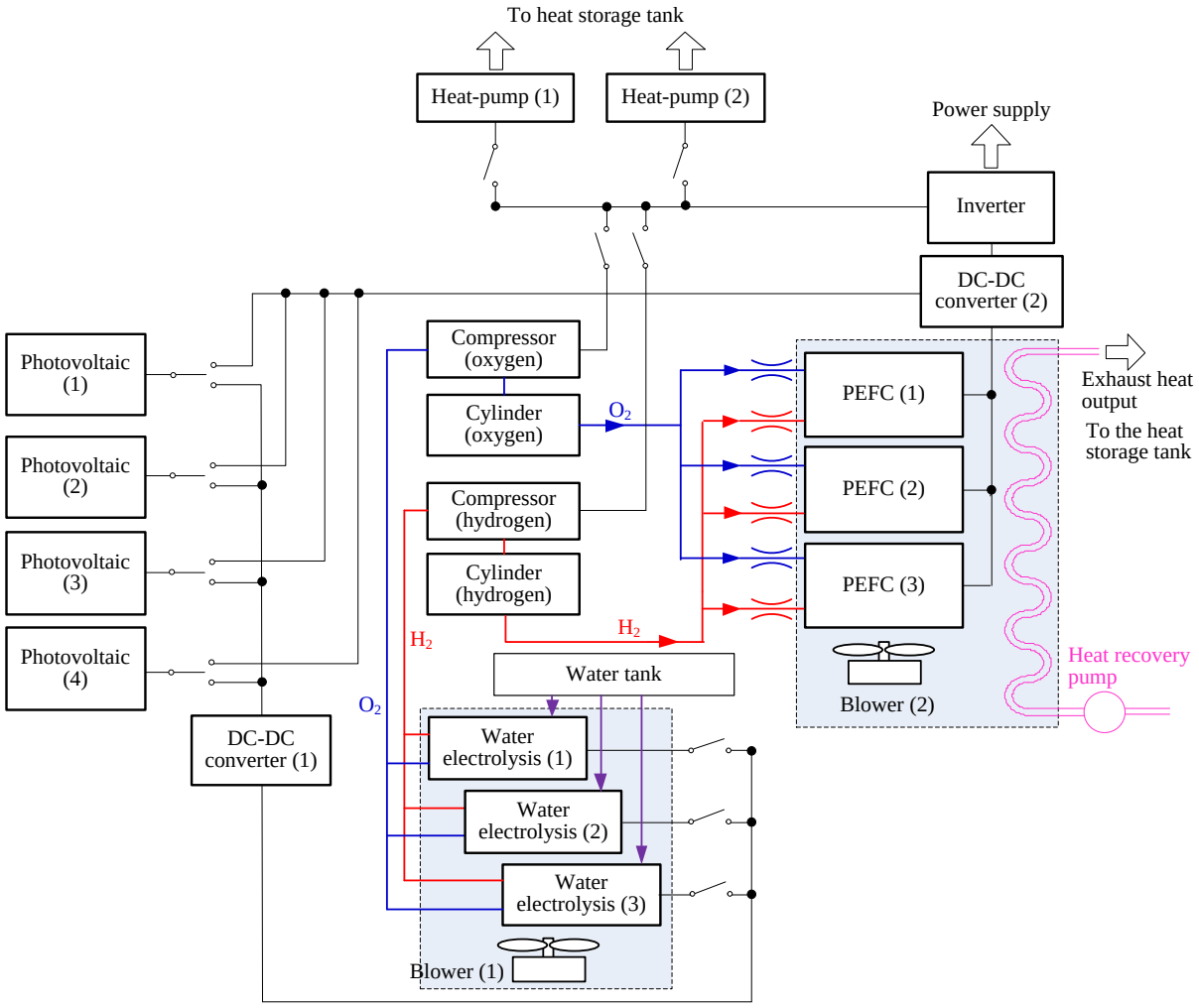

(a) Power system

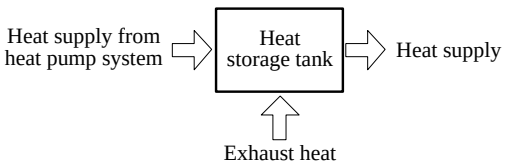

(b) Heat system

Fig. 1 System outline

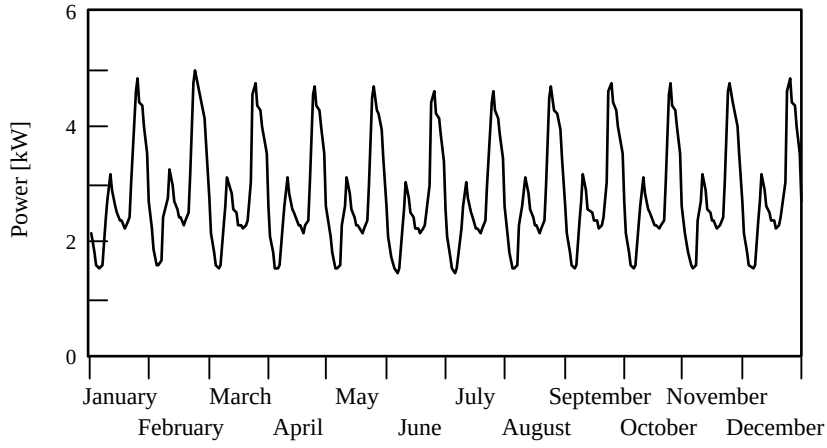

(a) Power

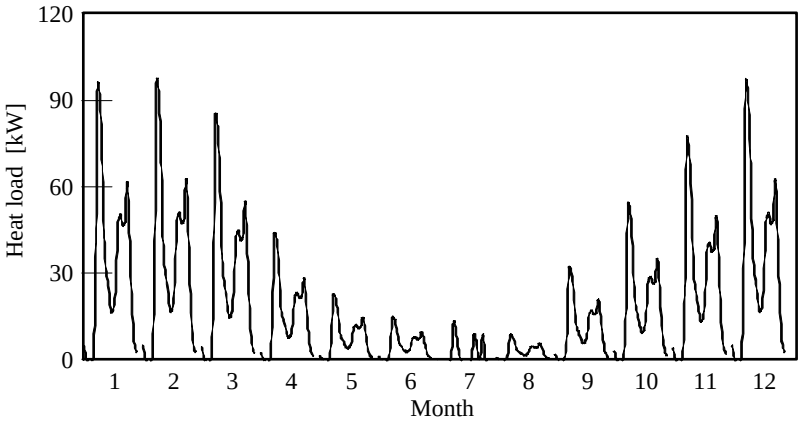

(b) Heat

Fig. 2 Power and heat demand model of six houses in Sapporo, Japan

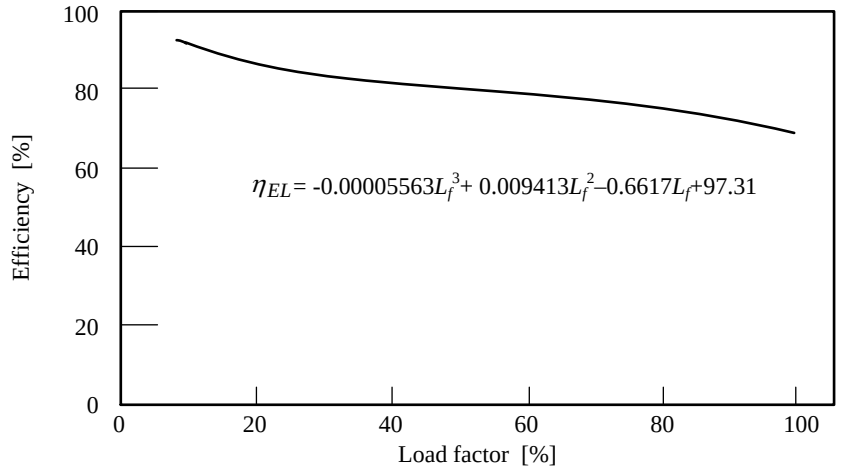

(a) Efficiency of the water electrolyzer

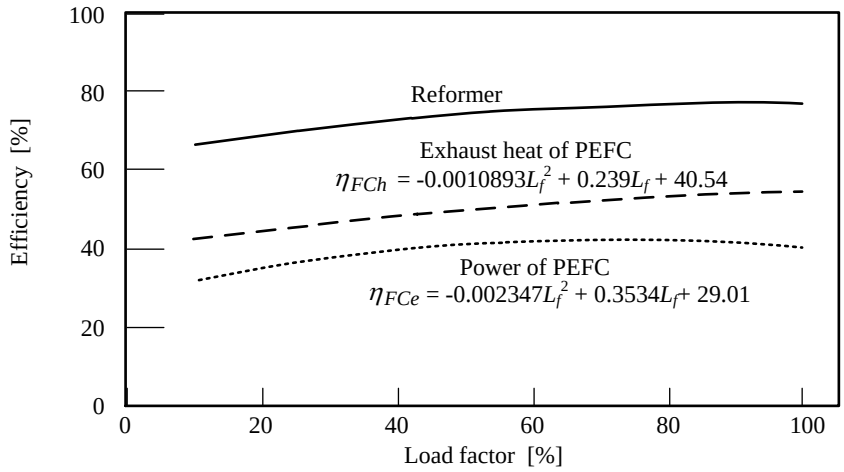

(b) Efficiency of the PEFC

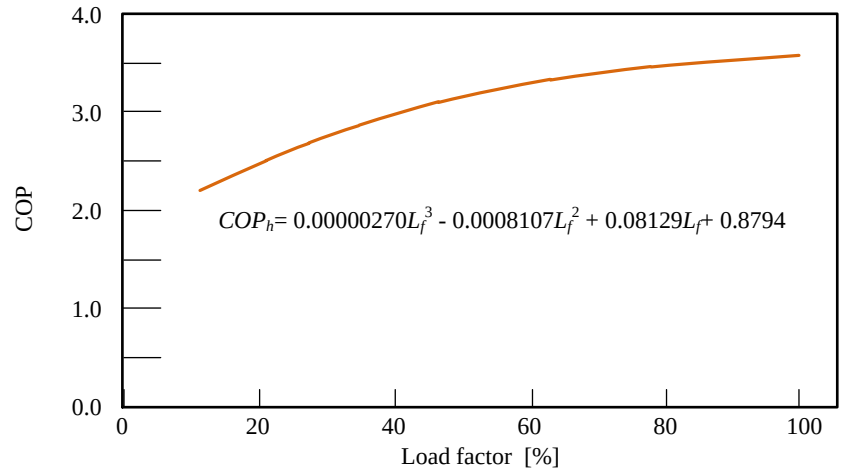

(c) COP of the heat pump

Fig. 3 Characteristics of each component

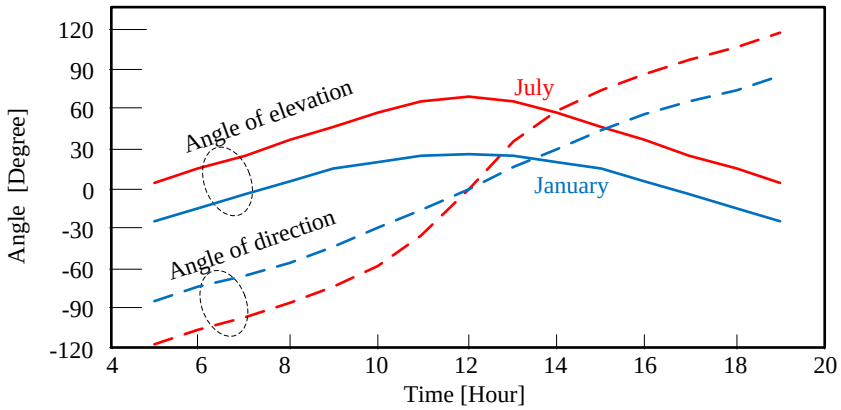

(a) The direction of the solar angle and elevation

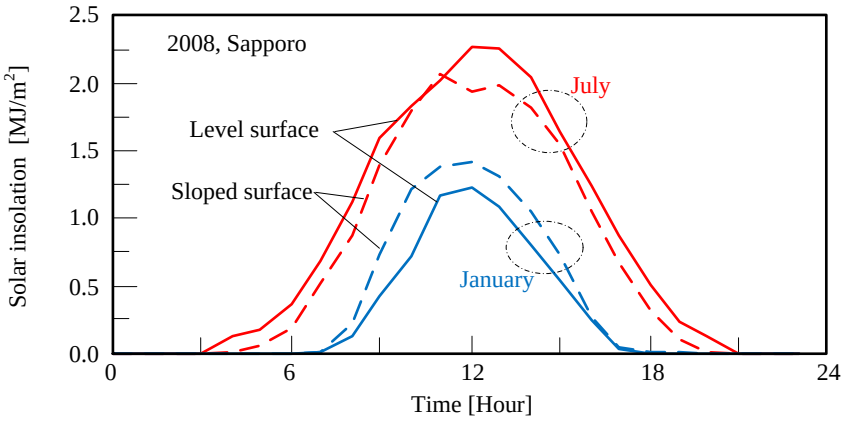

(b) Solar insolation

Fig. 4 Insolation of the level surface in Sapporo

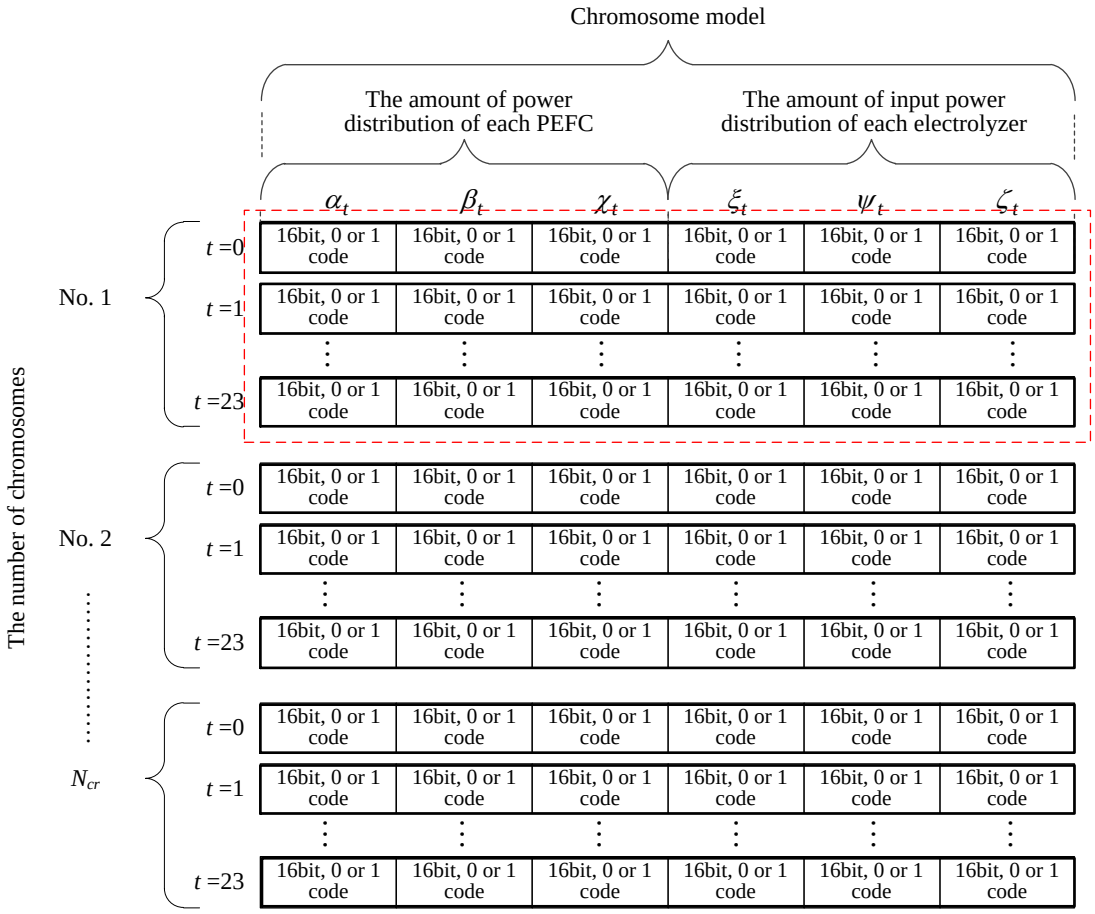

Fig. 5 Chromosome model using GA

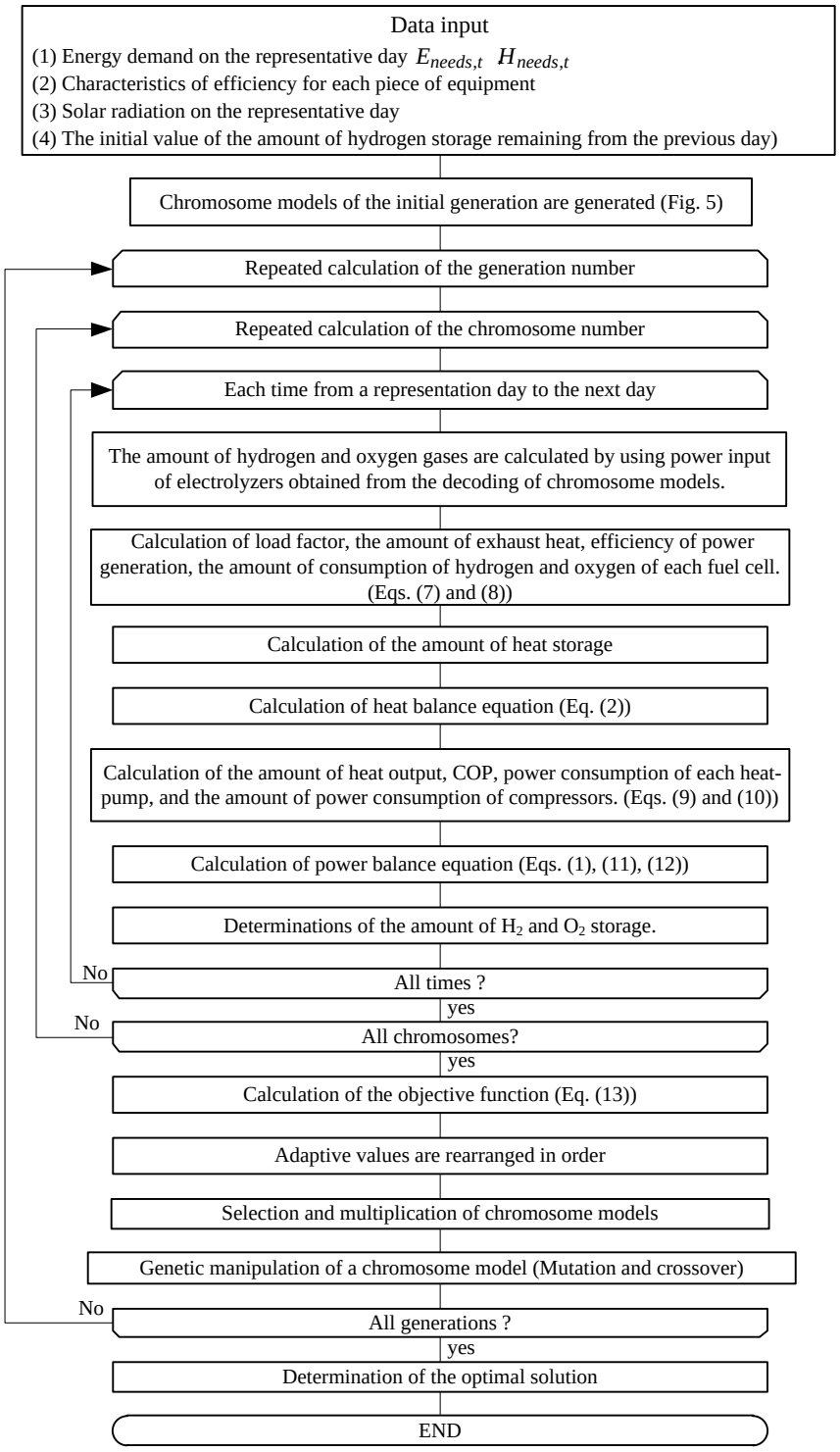

Fig. 6 Analysis flow using GA

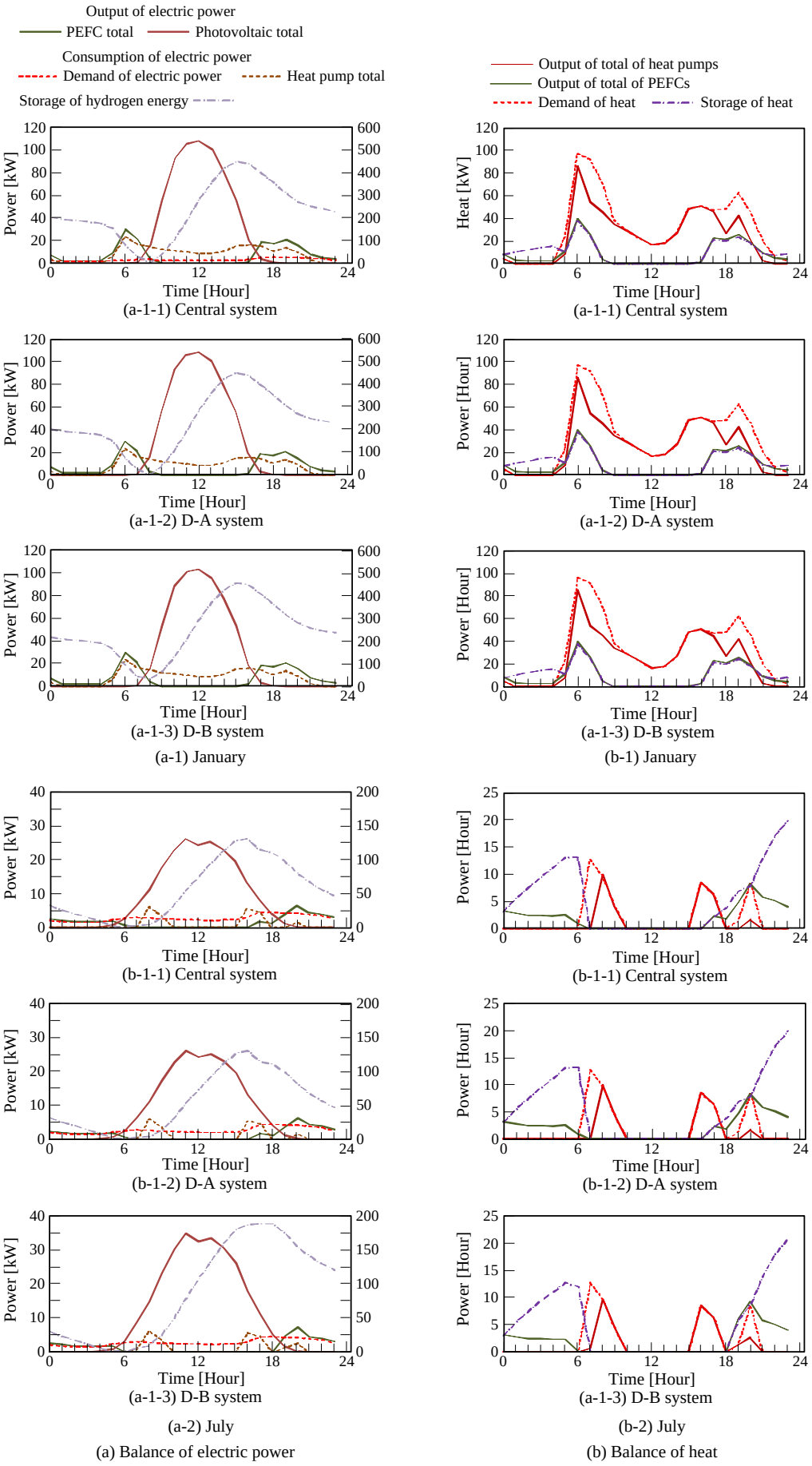

Fig. 7 Analysis results of the energy balance of the system

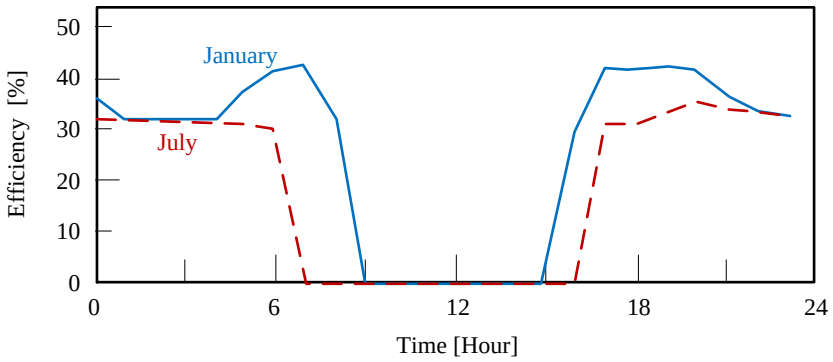

(a) Fuel cell

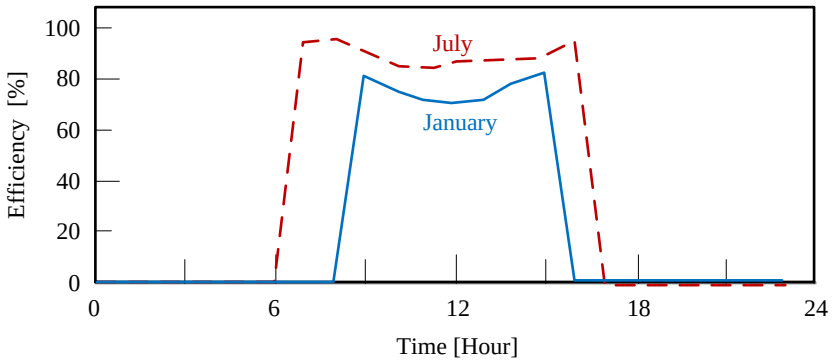

(b) Electrolyzer

Fig. 8 Analysis results of efficiency in centralized system

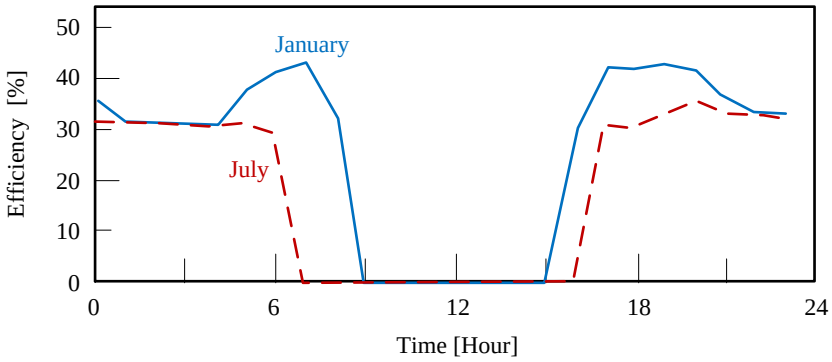

(a) Fuel cell

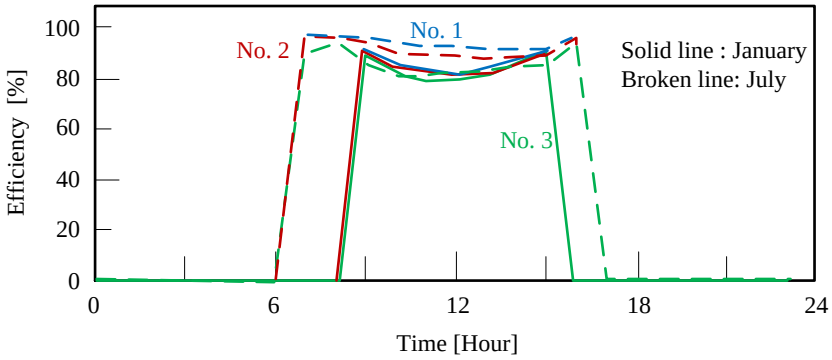

(b) Electrolyzer

Fig. 9 Analysis results of the efficiency of the D-A system

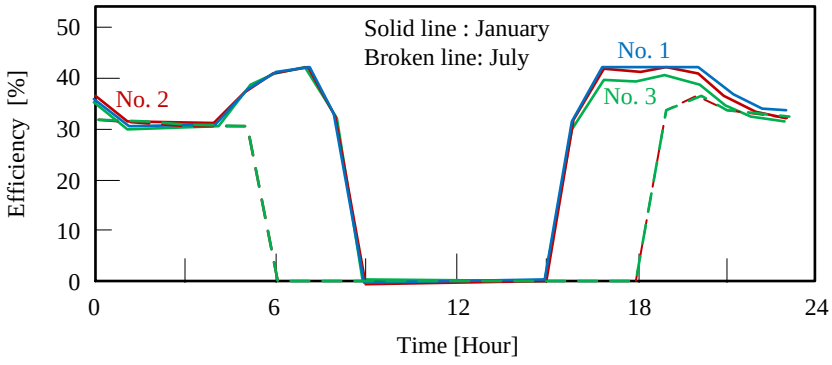

(a) Fuel cell

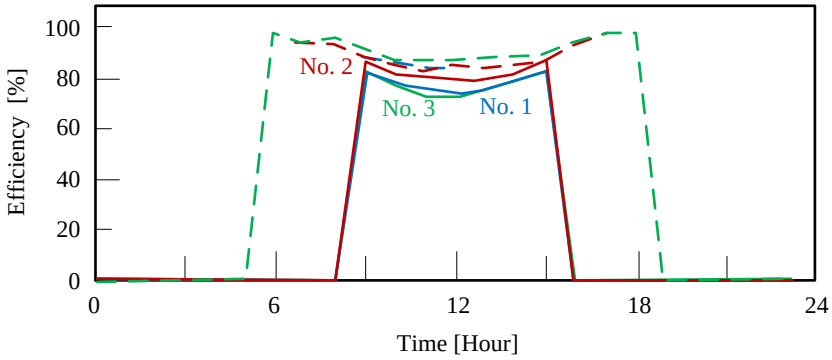

(b) Electrolyzer

Fig. 10 Analysis results of the efficiency of the D-B system

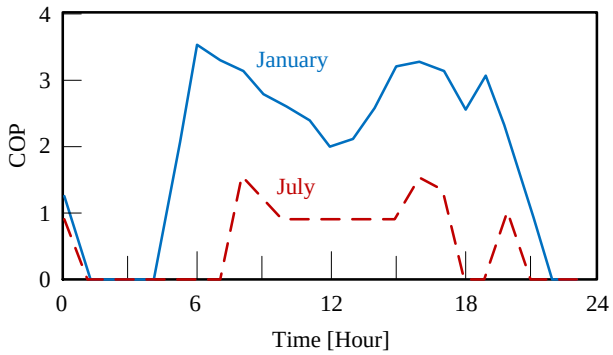

(a) Central system

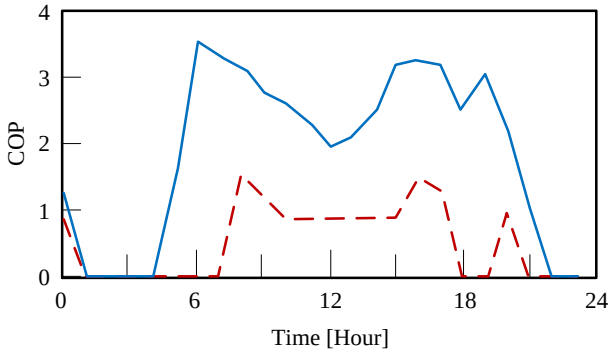

(b) D-A system

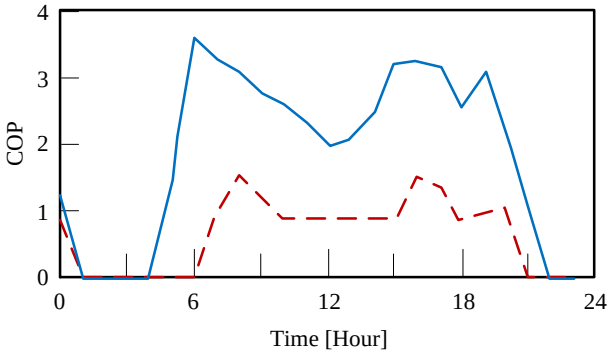

(c) D-B system

Fig. 11 The COP results of the heat pumps

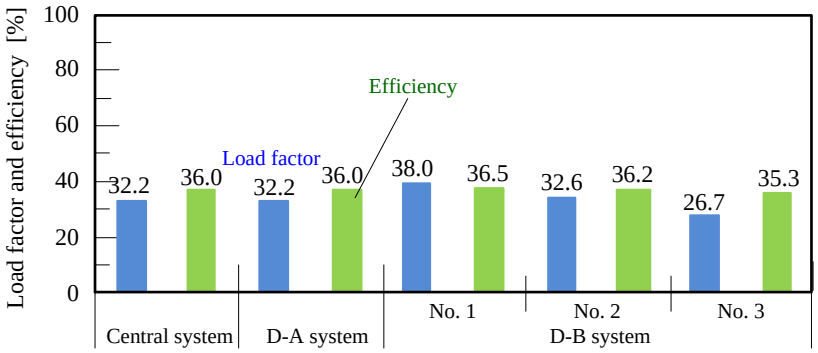

(a) January

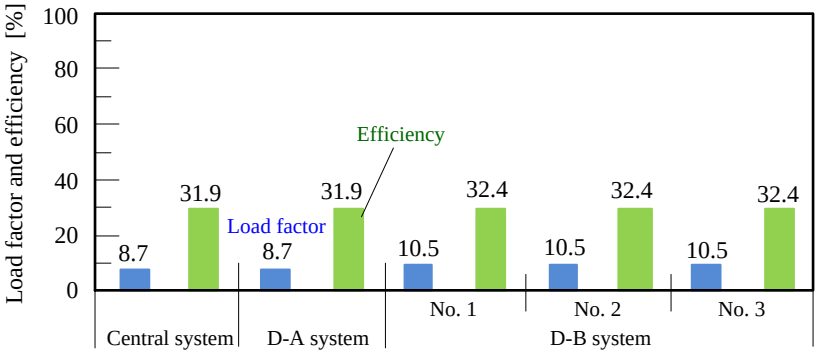

(b) July

Fig. 12 Analysis results of the fuel cell

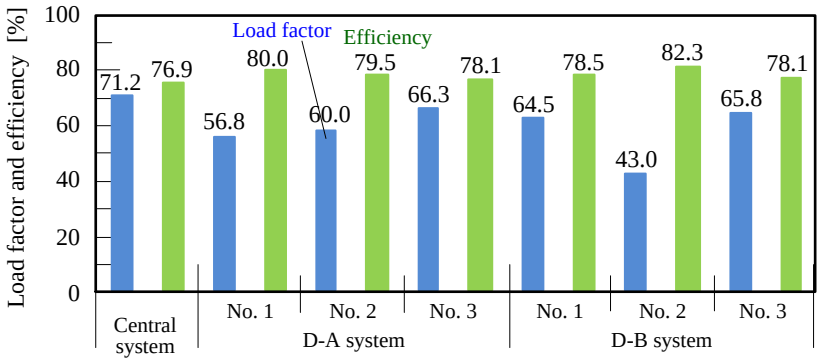

(a) January

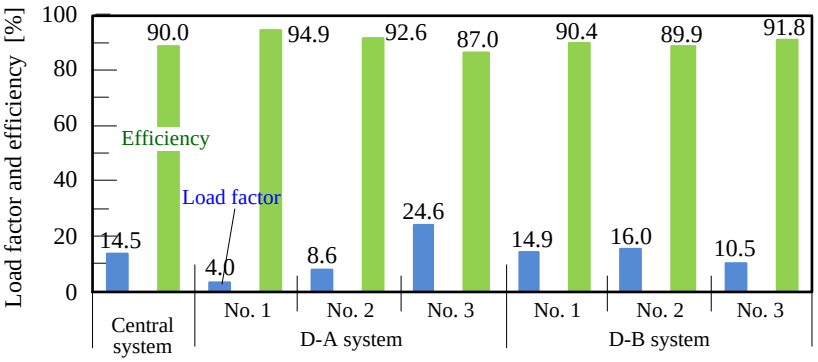

(b) July

Fig. 13 Analysis results of the electrolyzers

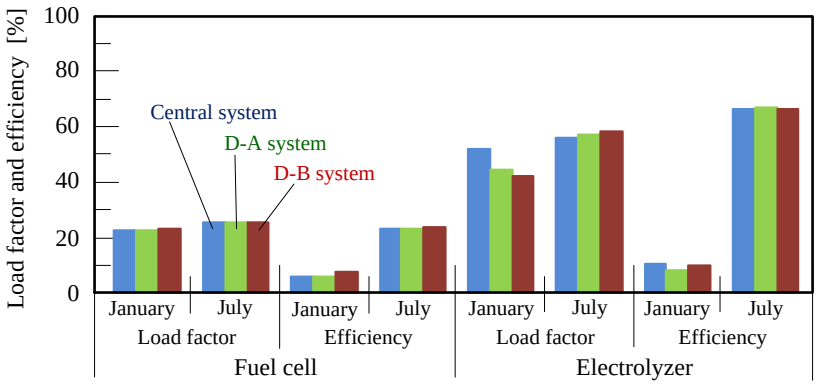

Fig. 14 Analysis results of the daily average

Table 1 Computation equations used for analysis

1. In the case of $H_{HST,t} > H_{needs,t}$

(1) In the case of $\sum_{j=1}^{N_{PV}} E_{PV,j,t} > E_{needs,t} + \sum_{n=1}^{N_{BW}} E_{BW,n,t}$

a. $\sum_{k=1}^{N_{EL}} E_{EL,k,t} = \sum_{j=1}^{N_{PV}} E_{PV,j,t} - \left(E_{needs,t} + \sum_{n=1}^{N_{BW}} E_{BW,n,t} \right)$

b. $\sum_{i=1}^{N_{FC}} E_{FC,i,t} = 0$

c. $H_{HST,t} = H_{HST,t-1} - H_{needs,t}$

d. $Q_{H_2ST,t} = Q_{H_2ST,t-1} + \sum_{k=1}^{N_{EL}} Q_{EL,k,t} = 0$

e. $\sum_{j=1}^{N_{HP}} H_{HP,j,t} = 0$

(2) In the case of $\sum_{j=1}^{N_{PV}} E_{PV,j,t} \le E_{needs,t} + \sum_{n=1}^{N_{BW}} E_{BW,n,t}$

a. $\sum_{k=1}^{N_{EL}} E_{EL,k,t} = 0$

b. $\sum_{i=1}^{N_{FC}} E_{FC,i,t} = E_{needs,t} + \sum_{n=1}^{N_{BW}} E_{BW,n,t} - \sum_{j=1}^{N_{PV}} E_{PV,j,t}$

c. $H_{HST,t} = H_{HST,t-1} - H_{needs,t} + \sum_{i=1}^{N_{FC}} H_{FC,i,t}$

d. $Q_{H_2ST,t} = Q_{H_2ST,t-1} - \sum_{i=1}^{N_{FC}} Q_{FC,i,t} = 0$

e. $\sum_{j=1}^{N_{HP}} H_{HP,j,t} = 0$

2. In the case of $H_{HST,t} \le H_{needs,t}$

(1) In the case of $\sum_{j=1}^{N_{PV}} E_{PV,j,t} > E_{needs,t} + \sum_{n=1}^{N_{BW}} E_{BW,n,t}$

In the case of $\sum_{j=1}^{N_{HP}} H_{HP,j,t} \ge H_{needs,t} - H_{HST,t-1}$

a. In the case of $\sum_{j=1}^{N_{PV}} E_{PV,j,t} > E_{needs,t} + \sum_{n=1}^{N_{BW}} E_{BW,n,t} + \sum_{l=1}^{N_{HP}} E_{HP,l,t}$

- $\sum_{k=1}^{N_{EL}} E_{EL,k,t} = \sum_{j=1}^{N_{PV}} E_{PV,j,t} - \left(E_{needs,t} + \sum_{n=1}^{N_{BW}} E_{BW,n,t} + \sum_{l=1}^{N_{HP}} E_{HP,l,t} \right)$
- $\sum_{i=1}^{N_{FC}} E_{FC,i,t} = 0$
- $H_{HST,t} = 0$
- $Q_{H_2ST,t} = Q_{H_2ST,t-1} - \sum_{k=1}^{N_{EL}} Q_{EL,k,t}$

b. In the case of $\sum_{j=1}^{N_{PV}} E_{PV,j,t} \le E_{needs,t} + \sum_{n=1}^{N_{BW}} E_{BW,n,t} + \sum_{l=1}^{N_{HP}} E_{HP,l,t}$

- $\sum_{k=1}^{N_{EL}} E_{EL,k,t} = 0$
- $\sum_{i=1}^{N_{FC}} E_{FC,i,t} = E_{needs,t} + \sum_{n=1}^{N_{BW}} E_{BW,n,t} + \sum_{l=1}^{N_{HP}} E_{HP,l,t} - \sum_{j=1}^{N_{PV}} E_{PV,j,t}$
- $H_{HST,t} = \sum_{i=1}^{N_{FC}} H_{FC,i,t}$
- $Q_{H_2ST,t} = Q_{H_2ST,t-1} - \sum_{i=1}^{N_{FC}} Q_{FC,i,t}$

(2) In the case of $\sum_{j=1}^{N_{PV}} E_{PV,j,t} \le E_{needs,t} + \sum_{n=1}^{N_{BW}} E_{BW,n,t}$

a. $\sum_{j=1}^{N_{HP}} H_{HP,j,t} = H_{needs,t} - H_{HST,t-1}$

b. $\sum_{i=1}^{N_{FC}} E_{FC,i,t} = E_{needs,t} + \sum_{n=1}^{N_{BW}} E_{BW,n,t} + \sum_{l=1}^{N_{HP}} E_{HP,l,t} - \sum_{j=1}^{N_{PV}} E_{PV,j,t}$

c. $\sum_{k=1}^{N_{EL}} E_{EL,k,t} = 0$

d. $H_{HST,t} = \sum_{i=1}^{N_{FC}} H_{FC,i,t}$

e. $Q_{H_2ST,t} = Q_{H_2ST,t-1} - \sum_{i=1}^{N_{FC}} Q_{FC,i,t}$

Table 2 Specification of each component

Photovoltaics	4 sets	Heat storage tank	
Area of solar cell	Variable	Heat storage efficiency ($\eta_{HST,in}$)	95 %
Efficiency	20 %	Heat output efficiency ($\eta_{HST,out}$)	95 %
Fuel cell (PEFC)	1 or 3 sets	Compressor (H_2 and O_2)	1 set
Efficiency	Fig. 3 (b)	Compressed pressure (P_{CP,H_2})	1 MPa
Total capacity	30 kW	Efficiency (η_{CP})	60 %
Electrolyzer (proton-exchange type)	1 or 3 sets	Inverter ($\eta_{it,1}$, $\eta_{it,2}$)	95 %
Efficiency	Fig. 3 (a)	DC-DC converter (η_{dc1} , η_{dc2})	95 %
Total capacity	105 kW	Blower (E_{BW})	50 W
Heat-pump	2 sets		
COP	Fig. 3 (c)		
Capacity	50 kW each		

Table 3 Parameters of GA

The number of generations	50
The number of chromosomes	10000
Probability of cross over	50 %
Probability of mutation	80 %
Chromosome model (Individual)	Fig. 5